Construction and Building Materials 240 (2020) 117898

Contents lists available at ScienceDirect

Construction and Building Materials

journal homepage: www.elsevier.com/locate/conbuildmat

The expansion behavior of slurries containing recycled glass powder carboxymethyl cellulose, lime and aluminum powder

Doğuş Zeren [a], Ufuk Şentürk [a], Mustafa Güden [b,*]

[a] Department of Materials Science, Izmir Institute of Technology, Gülbahçe Köyü, Urla, Izmir, Turkey
[b] Department of Mechanical Engineering, Izmir Institute of Technology, Gülbahçe Köyü, Urla, Izmir, Turkey

HIGHLIGHTS

- Glass foams made of recycled glass, cellulose, lime and aluminum powder slurries.
- The viscosity significantly affected the expansion behavior of the slurries.
- Average densities: 355–530 kg m^{-3} and average compressive strengths: 0.2–0.5 MPa.
- Increasing sintering time to 60 min increased the compressive strength to 1.5 MPa.
- Lower compressive strength and thermal conductivities due to cell wall pores.

ARTICLE INFO

Article history:
Received 30 July 2019
Received in revised form 10 November 2019
Accepted 17 December 2019
Available online 28 December 2019

Keywords:
Glass
Powder
Foam
Aluminum
Sintering
Compressive strength
Thermal conductivity

ABSTRACT

The rheology and foaming/expansion of the slurries of a waste/recycled glass powder with 50, 55 and 60 wt% of solid (glass powder) were experimentally investigated. The glass powder slurries were foamed using aluminum powder as foaming agent (0.75 wt%) and calcium hydroxide as activator (1 wt%). Sodium carboxymethyl cellulose (CMC) was added to the slurries as a binder with the amounts between 0 and 4 wt%. The expansions of the slurries were measured in-situ using a laser sensor and reported as percent volume expansion. The CMC-addition increased the viscosities of the slurries, particularly the fine size powder slurries. The slurries with the relatively low-viscosity exhibited lower initial expansion rates compared to the slurries with the relatively high-viscosity. The maximum expansions of the slurries increased from 300 to 350%, when the viscosity increased to 5 Pa s and reached a steady value around 400% between 5 and 50 Pa s. The expansions of the slurries could not be achieved above 50 Pa s since they became too thick to be foamed. The foam samples made from the slurries with 55 and 60 wt% of solid and sintered at 700 and 750 °C for 30 min had the average densities between 355 and 530 kg m^{-3} and the average compressive strengths between 0.2 and 0.5 MPa. Increasing sintering time to 60 min at 750 °C increased the average compressive strength from 0.5 to 1.5 MPa for the foam samples made from the slurry with 60 wt% of solid. These proved that both sintering temperature and time were effective in increasing the compressive strengths of the foamed structures. The thermal conductivities of the sintered foam samples with the densities of 355 and 504 kg m^{-3} were measured 0.042 and 0.057 W m^{-1} K^{-1}, respectively.

1. Introduction

Glass foams exhibit relatively high compressive strength, low thermal conductivity, high sound absorption, low moisture absorption, non-flammability and high freeze-thaw resistance. The combinations of above properties make them suitable for the heat and sound insulations of buildings, pipes and etc. The methods of glass foam processing by incorporating a gas evolving substance (foaming agent) into a molten glass and by mixing the foaming agent with a glass powder followed by heating the powder mixture to the softening point of glass were patented as early as 1934 and 1938, respectively [1,2]. The current glass foam production is largely based on foaming waste/recycled-glass powder in the presence of a foaming agent at a relatively high temperature [3]. In this process, the waste-glass powder precursor mixed with a foaming agent is heated to the softening point of glass and the gas

* Corresponding author at: Izmir Institute of Technology, Gulbahce Koyu, Urla, Izmir 35430, Turkey.
E-mail address: mustafaguden@iyte.edu.tr (M. Güden).

https://doi.org/10.1016/j.conbuildmat.2019.117898
0950-0618/

released by the decomposition/reaction of the foaming agent expands softened glass powder body. The foaming agents used in above process are classified as *neutralizers*: $CaCO_3$ [4–6], $CaMg(CO_3)_2$ [7], Na_2CO_3 [8,9] and MnO_2 [10,11] and *redox* agents: C [12], SiC [5,13–19], Si_3N_4 [17,20], AlN [17] and TiN [13]). Neutralizers decompose upon heating, releasing CO_2, while redox agents react with glass, forming CO_2, CO or N_2, depending the type of the foaming agent used.

The main drawback of the glass foam processing based on the foaming glass powders at an elevated temperature with the use of a foaming agent is the comparably high unit cost. In addition, glass foams have an approximately 20% higher thermal conductivity than polystyrene foams and mineral fibers [11]. Soda-lime-silicate and cathode-ray-tube glass foaming were accomplished at 750–950 °C using $CaCO_3$ [21,22] and 950 °C using SiC foaming agents [23]. Furthermore, $CaCO_3$ reacts with glass melt at the surface, making foaming process difficult to control [4,24,25]. The melt viscosity window of foaming soda-lime-silicate and cathode-ray-tube glasses for achieving minimum final foam densities was determined between 10^4–10^6 Pa s using carbonates and $10^{3.3}$–10^4 Pa s using SiC [24]. As the melt viscosity is affected by the temperature, heating rate, crystallization of melt and surface chemistry, the adjustment of viscosity becomes complicated. Glass foams are however environmentally friendly in production and usage [26]; therefore, the market size has been steadily growing in all countries over the past two decades [11]. According to authors' investigation, there appeared approximately 170 scientific articles in Web of Science on glass foams; however, the total number of patents related to manufacturing was 390 until 2015, which implied the importance of need for new methods. In the period of 1930–2015, total 161 patents were published by the USA, 135 patents by China, 31 patents by European countries, 25 patents by Japan and 38 by Russia. The patent publications by China started in 1990s and gained an increase after 2000s.

In present study, the feasibility of glass foam processing by expanding at room temperature the slurries of a waste/recycled glass powder and by sintering the expanded bodies at elevated temperatures was investigated experimentally. The slurries in different powder size and wt% of solid and binder were prepared and expanded with the addition of an aluminum powder (foaming agent) and a $Ca(OH)_2$. $Ca(OH)_2$ is a widely used alkali activator in processing autoclaved aerated concretes [27–30]. The compressive strengths and thermal conductivities of the sintered foam samples were determined and compared with those of the published in the literature. Based on authors' knowledge, there has been only one study [31] in the literature on the expanded powder slurries (fly ash slurries with the addition of glass powder addition) to form solid foam structures. The studied method hence gives a new insight for foam glass processing and can also potentially eliminate the difficulties of controlling process parameters of the conventional high-temperature foam glass processing method.

2. Materials and experiments

Recycled soda-lime-silica glass powder was obtained from a local supplier with an average particle size of ~72 μm (Malvern Mastersizer 2000). The elemental composition of the as-received glass powder was determined 73% SiO_2, 12% Na_2O, 12% CaO, 1.6% MgO and 1.4% Al_2O_3 (Spectro IQ II X-Ray Fluorescence). The as-received glass powder particles had angular shapes with relatively low aspect ratios as seen in Fig. 1(a) (FEI Quanta 205 FEG and Philips XL 30SFEG SEM). The powder was fractioned using a Fritsch Analtysette 3 PRO type vibrational screener into three sieve sizes: below 38 μm (fine), between 38 and 45 μm (medium) and between 45 and 56 μm (coarse). The softening point of the used glass powder was previously measured ~680 °C [19]. A commercially available aluminum powder (0.75 wt%) and a $Ca(OH)_2$ powder (1 wt %), both supplied by AKG Gazbeton company of Turkey, were used as the foaming agent and activator, respectively. The flake-shape aluminum particles of the foaming agent had the lengths of long-axis between 25 and 50 μm and short-axis in few micrometers as seen in Fig. 1(b). Sodium carboxymethyl cellulose (Sigma Aldrich 419273) was used as a binder in the slurries with 0, 2, 3 and 4 wt% to achieve a green strength of dried foams. The rheology of the slurries was determined using a Thermo Electron Corporation Haake Mars II Rotational Rheometer device. The investigated fine, medium and coarse glass powder slurries are tabulated in Table 1.

The slurries were prepared by mixing glass powder (50, 55 and 60 wt%) with lime and CMC in distilled water for a few minutes at 2000 rpm. After adding aluminum powder, the slurry was mixed for 15 s at 2000 rpm and then poured into a 40 mm-diameter cylindrical Teflon tube (Fig. 2(a)). Teflon tube was used to reduce the frictional forces between the slurry and the mold. Few foaming experiments were conducted inside a transparent Plexiglas tube in order to video-record the bubble evolution as function of time (Fig. 2(b)).

The experimental set-up used in the expansion experiments is shown in Fig. 3. A laser displacement sensor (Micro Epsilon ILR1030-8) clamped by a holder at a distance of 20 cm above the

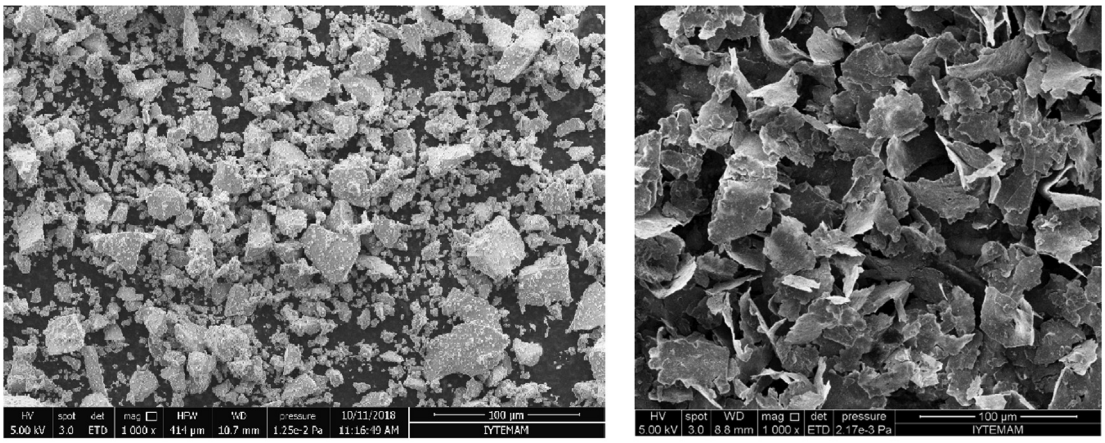

Fig. 1. The SEM pictures of a) as-received glass powder and b) Al powder.

Table 1
The codes and measured viscosities of the slurries investigated.

Slurry	Viscosity 1 (Pa s)	Viscosity 2 (Pa s)	Viscosity 3 (Pa s)	Average Viscosity (Pa s)
Fine, 50 wt% solid, 2 wt% CMC	0.1	0.1	0.13	0.11
Fine, 60 wt% solid, 2 wt% CMC	1.36	1.35	1.3	1.34
Medium, 50 wt% solid, 2 wt% CMC	0.1	0.1	0.1	0.10
Medium, 60 wt% solid, 2 wt% CMC	1.36	1.35	1.3	1.34
Coarse, 50 wt% solid, 2 wt% CMC	1.1	1.06	1.06	1.07
Coarse, 60 wt% solid, 2 wt% CMC	0.24	0.24	0.25	0.24
Fine, 50 wt% solid, 3 wt% CMC	2.88	2.62	2.47	2.66
Fine, 60 wt% solid, 2 wt% CMC	4.59	4.21	4.07	4.29
Medium, 50 wt% solid, 3 wt% CMC	3.65	3.49	3.45	3.53
Medium, 60 wt% solid, 3 wt% CMC	4.93	4.73	4.73	4.80
Coarse, 50 wt% solid, 3 wt% CMC	1.08	1.08	1.08	1.08
Coarse, 60 wt% solid, 3 wt% CMC	1.66	1.67	1.67	1.67
Medium, 50 wt% solid, 4 wt% CMC	6.41	6.3	6.19	6.30
Medium, 60 wt% solid, 4 wt% CMC	28.7	18.2	18.2	21.70
Coarse, 50 wt% solid, 4 wt% CMC	3.42	3.26	3.34	3.34
Coarse, 60 wt% solid, 4 wt% CMC	6.48	5.36	5.74	5.86

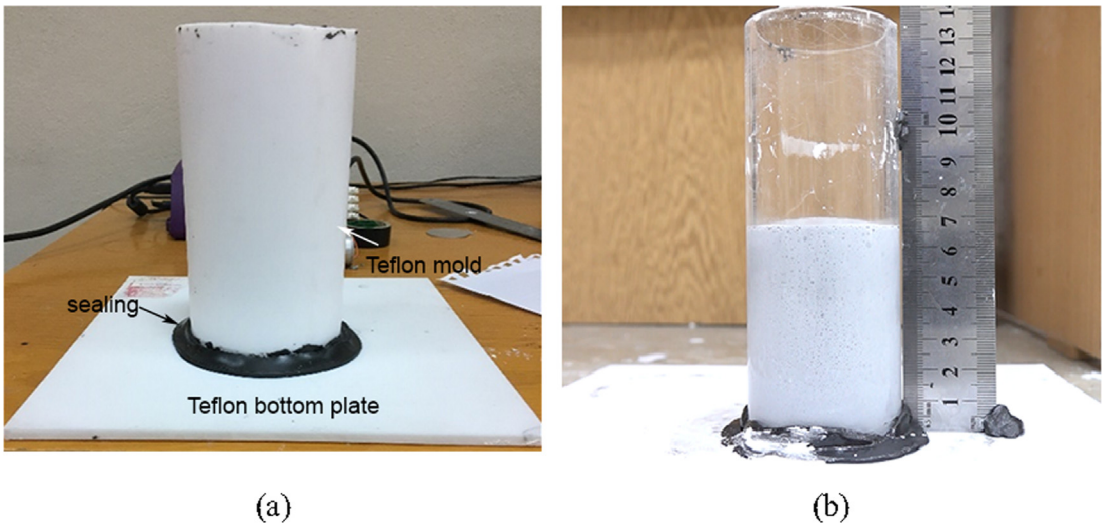

Fig. 2. Foaming molds a) Teflon© and b) transparent Plexiglas.

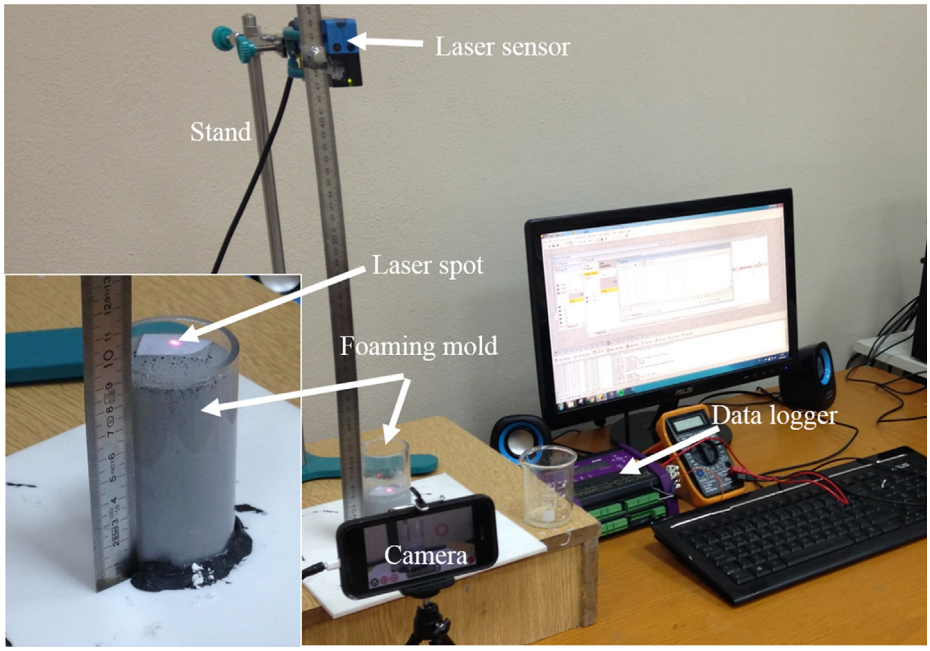

Fig. 3. Foam expansion experimental set-up.

foaming mold was sued to measure the expansions of the slurries in-situ as function of time. The sensor was operated between 4 and 20 mA and calibrated before each experiment by determining the corresponding current difference of a known distance. A piece of white paper was placed on the surface of the slurries before the start of the expansion measurement to provide a contrast background for the laser spot (Fig. 3). The simultaneous change in the expansions was recorded by a Data Taker DT 80 logger. The percent volume expansion (V_E) or linear expansion was calculated using the following relation

$$V_E(\%) = \frac{h_f - h_0}{h_0} \times 100 \quad (1)$$

where, h_f and h_o are the final and initial height of the slurry, respectively. Expansion experiments for each slurries were conducted in triplicate to determine a representative behavior. Pictures were taken during foaming in the Plexiglas mold at 420, 360, 720, 1200 and 1800 s (7, 9, 12, 20, and 30 min) using a Sony RX100ii high resolution camera. Since the bubble sizes were very small at the beginning of the foaming, they could not be detected until about 420 s.

Foamed slurries were dried at room temperature for 24 h; thereafter, sintered in a Protherm Laboratory Furnace Model PLF 130/25 at 650, 700, 750 and 800 °C with a heating rate of 10 °C min^{-1} for 30 min. The foam samples for the compression and thermal conductivity tests were expanded inside a larger-diameter plastic mold (75 mm). Following the sintering, the cylindrical compression test samples, 20 mm in diameter and 20 mm in length, were core-drilled through the foaming direction. The surfaces of core-drilled samples were cleaned by applying pressurized air. Before the compression test, the end surfaces of the samples were grounded flat. The density of each test sample was determined by dividing the weight by the volume of the sample. The tests were conducted in a displacement-controlled SHIMADZU AG-I universal test machine at a strain rate of 1×10^{-3} s^{-1} using axially self-aligned pin-ball compression test platens. At least 4 tests were performed for each group of samples and the resultant compressive strengths were averaged. Thermal conductivities of the diamond-saw-cut 30 × 10 × 10 mm size rectangular foam samples were measured in a C-Therm Thermal Conductivity Analyzer.

3. Results

3.1. Rheology of slurries

The shear stress-shear rate and viscosity-shear rate curves of the fine powder slurries with 50, 55 and 60 wt% of solid and 2 wt% of CMC content are shown in Fig. 4(a) and (b), respectively. Three separate measurements of the shear stress-shear rate of the slurries with 50 and 60 wt% of solid content in Fig. 4(a) are very similar to each other, proving the repeatability of the measurements. As is also noted in Fig. 4(b), the non-Newtonian behavior of the slurries with 50 and 55 wt% of solid content at low shear rates switches into the Newtonian behavior after ~20 s^{-1}, while the slurry with 60 wt% of solid content shows a non-Newtonian shear thinning. An increase in the wt% of solid content promotes a non-Newtonian behavior. The viscosities of the investigated slurries were determined at 20 s^{-1} and are tabulated in Table 1. Fig. 5 (a), (b) and (c) show sequentially the variations of the average viscosities of the fine, medium and coarse powder slurries with the wt % of CMC. As seen in the same figures, an increase in the wt% of CMC increases the viscosity of the slurries, while the increase in viscosity is more noticeable in the fine powder slurries, particularly with 4 wt% of CMC addition.

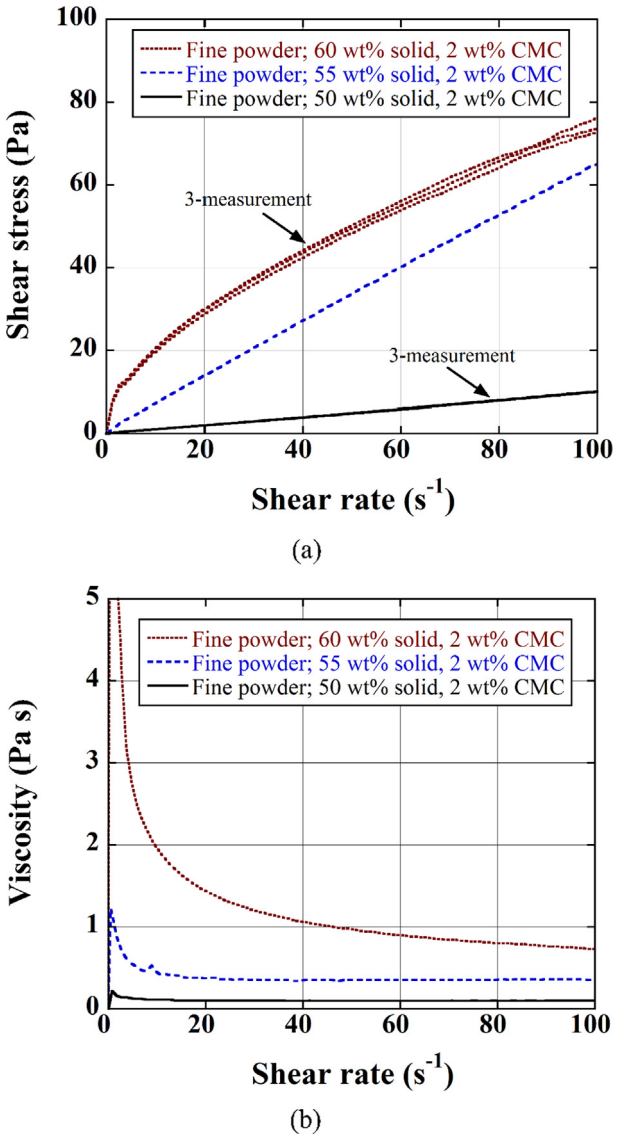

Fig. 4. (a) the shear stress-shear rate (3 tests for 50 and 60 wt% solid) and (b) viscosity-shear rate curves of the fine powder slurries with 50, 55 and 60 wt% solid and 2 wt% CMC content.

3.2. Foaming experiments

Fig. 6 shows the expansion-time curves of the medium size powder slurries with 50 and 55 wt% of solid and 4 wt% of CMC content. The pictures of the expanding slurries are also shown in the same figure at various times. The oscillations in the expansion-time curves are due to the electronic background noise of the laser sensor. The smoothed-expansion-time curves of the slurries with 50 and 55 wt% of solid are also shown in Fig. 6 with dashed lines, together with that of the slurry with 60 wt% of solid. The initial expansion of the slurries starts with the bubble nucleation and growth and proceeds with a high expansion rate until about a maximum expansion, ~700 s for 60 wt%, ~1000 s for 55 wt% and ~1500 s for 50 wt% of solid. The expansion rates of the slurries with 55 and 60 wt% of solid are very similar to each other in this stage, however, about 2.4 times that of 50 wt% solid slurry (Fig. 6). The expansions decrease after the maximum; the reduction is gradual in the slurry with 50 wt% of solid and the highest in the slurry with 60 wt% of solid.

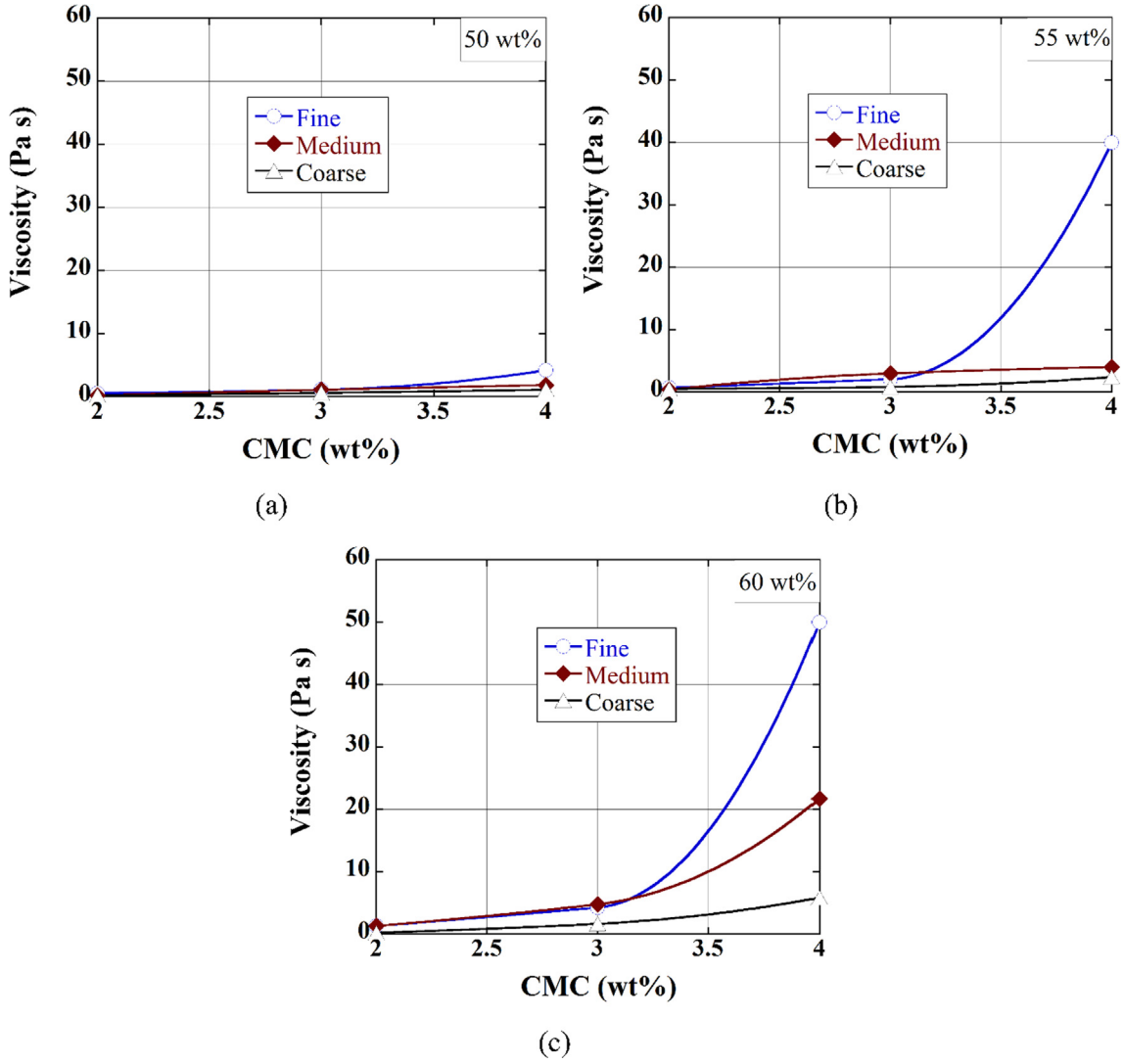

Fig. 5. The average viscosity vs. CMC-wt% of the slurries with (a) 50, (b) 55 and (c) 60 wt% solid.

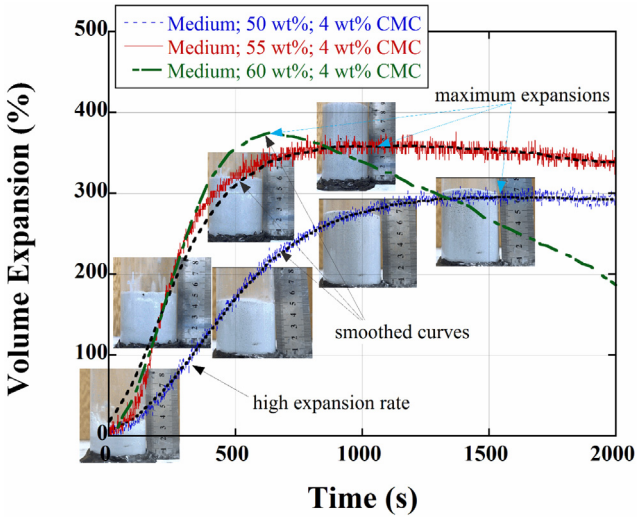

Fig. 6. The expansion-time curves of medium powder slurries with 50, 55 and 60 wt% of solid and 2 wt% of CMC addition together with the pictures of the Plexiglas foaming mold showing the expansions of slurries with 50 and 55 wt% of solid.

The representative expansion-time curves of the fine, medium and coarse powder slurries with different solid and CMC content are shown in Fig. 7(a-c), respectively. The arrows in the same figures show the wt% of solid and the numbers in the circles below the arrows show the corresponding wt% of CMC. In the same figures, the expansion-time curves of the slurries without CMC addition are also shown for comparison. As seen in the same figures, the expansions of all slurries with CMC addition increase over those without CMC addition. As is also seen in Fig. 7(a), increasing solid content from 50 to 55 and 60 wt% in the fine powder slurries increases the initial expansion rate. The expansions of the fine powder slurries with 55 and 60 wt% of solid content decrease more rapidly after the maximum expansion, while the decrease is more notable in the slurries with 60 wt% of solid. The expansion of the fine powder slurries with 50 wt% of solid slightly decreases, while the slurries with 55 wt% of solid increases with increasing the wt% of CMC from 2 and 4. A maximum expansion above 400% is seen in the fine powder slurries with 55 wt% of solid and 4 wt% of CMC, while the slurries with 60 wt% of solid and 4 wt% of CMC could not be foamed due to excessive increase in the viscosity. Increasing both the wt% of solid and CMC increases the maximum expansions in the medium powder slurries (Fig. 7(b)). A maximum expansion over 400% is seen in the medium powder slurries with 60 wt% of

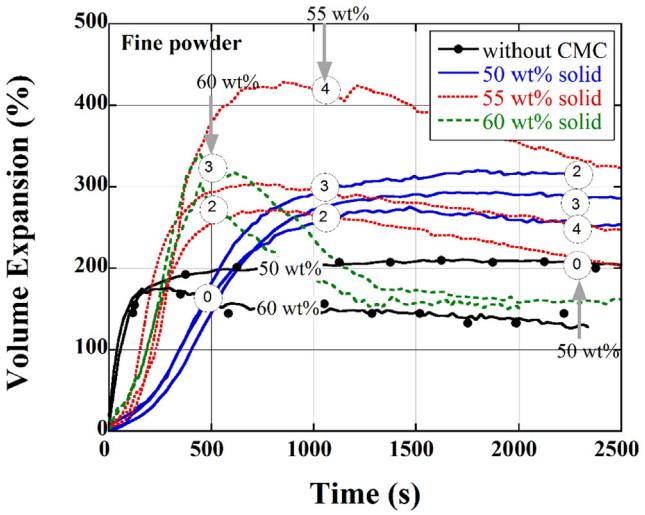

(a)

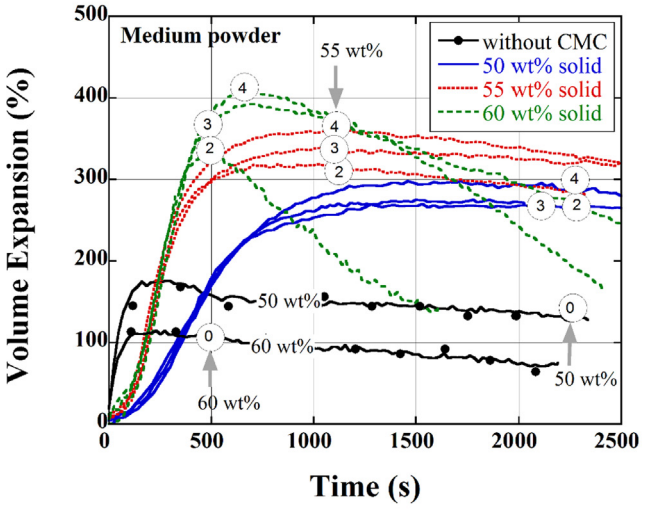

(b)

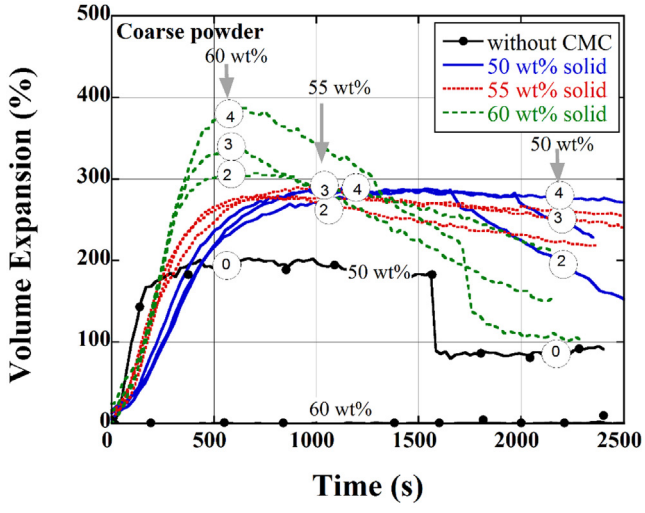

(c)

Fig. 7. The expansion-time curves of (a) fine, (b) medium and (c) coarse powder slurries with different wt% of solid and CMC addition.

solid and 4 wt% of CMC. Similar initial rapid expansions are also seen in all coarse size powder slurries regardless of the wt% of solid and CMC as seen in Fig. 7(c). The expansions of the coarse powder slurries with 50 and 55 wt% of solid are very much similar to each other; the maximum expansions are nearly 300% and increase slightly with increasing the solid content. The maximum expansions are however higher in the slurries with 60 wt% of solid, between 300 and 400%, but these values are lower than those of the fine and coarse size powder slurries at the same solid wt%. The expansions of the coarse size powder slurries also decrease after the maximum expansion, the degree of which increases with increasing the wt% of solid. Briefly, the fine size powder slurries with 55 wt% of solid and the medium and coarse size powder slurries with 60 wt% of solid at 4 wt% of CMC addition show the highest maximum expansions, while these slurries also exhibit rapid reductions in expansions after the maximum expansion.

The variation of the maximum expansions of the powder slurries with the logarithm of the apparent viscosity is shown in Fig. 8. The average maximum expansion of the slurries without CMC addition, ~200%, is also shown with a dashed line (Fig. 8). The addition of CMC increases the expansions from 200 to 300% in the low-viscosity slurries, ~0.22 Pa s. The maximum expansions increase moderately with increasing the viscosity from 0.22 to ~5 Pa s. However, the maximum expansions increase above 400% after a critical viscosity of ~5 Pa s. The maximum expansions remain almost constant until about ~50 Pa s, above which the slurries became too thick to be foamed.

3.3. Microstructure, compressive strength and thermal conductivity

Fig. 9(a) shows the picture of a foamed green body of the medium size powder slurry with 55 wt% of solid and 4 wt% of CMC, foamed inside the Teflon mold, and Fig. 9(b) shows an expanded powder slurry inside the rectangular plastic mold for the preparation of the compression and thermal conductivity test samples. Both, the compression and thermal conductivity test samples were cut normal to the foam expansion direction as shown by an arrow in the same figure. The fracture surface of a foamed and dried green body is shown in Fig. 10(a). Relatively homogenous interconnected cells in few millimeters size are seen in Fig. 10(a). The

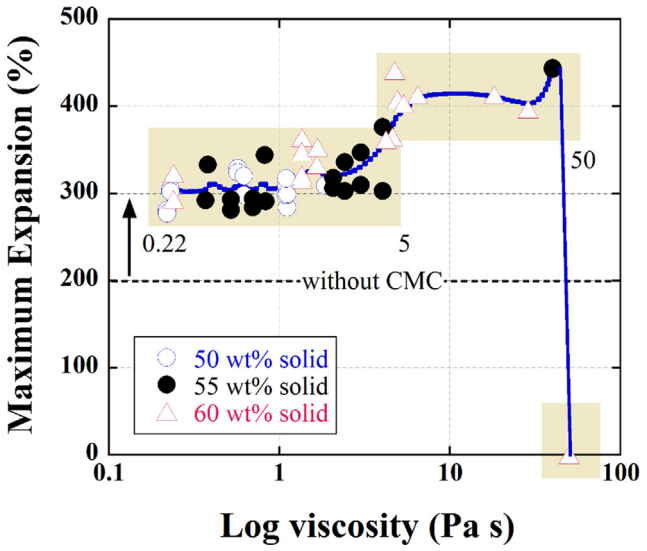

Fig. 8. The variation of maximum expansion with the logarithm of the viscosity.

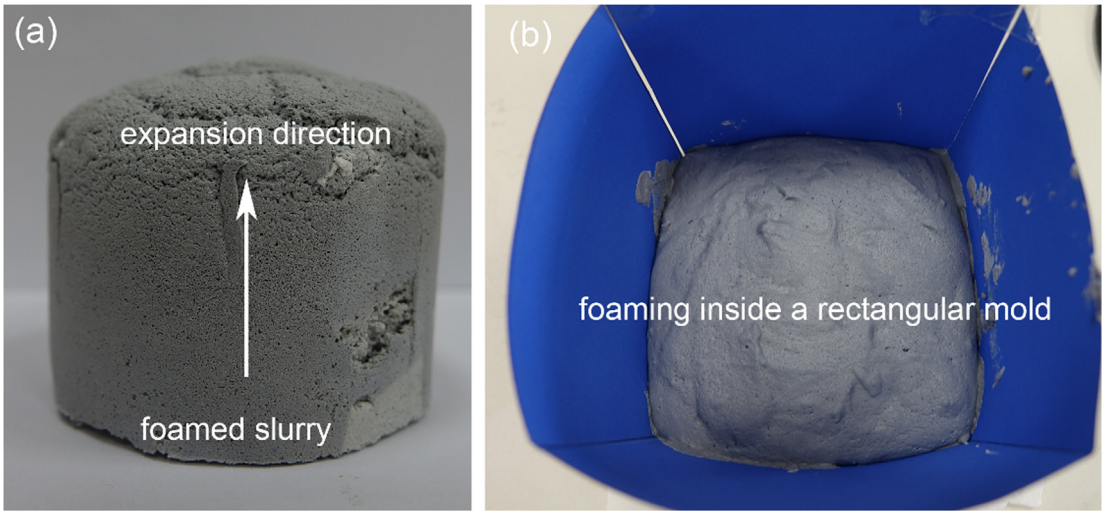

Fig. 9. (a) the picture of the foamed green body after removing from the Teflon tube (b) the picture of an expanding slurry in the rectangular plastic mold. (For interpretation of the references to colour in this figure legend, the reader is referred to the web version of this article.)

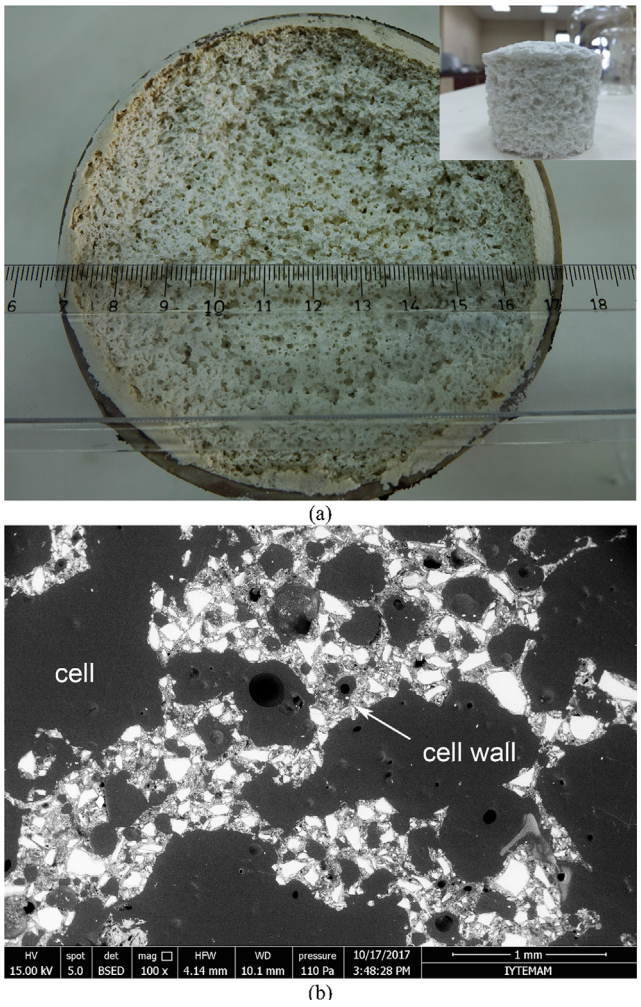

Fig. 10. (a) the picture of a foamed green body and (b) the SEM image of the polished surface of foamed green body embedded into the epoxy mold showing the glass particles on the cell walls. (For interpretation of the references to colour in this figure legend, the reader is referred to the web version of this article.)

SEM image of the epoxy-molded and polished cross-section of a foamed green body, normal to foam expansion direction, is shown in Fig. 10(b). In this micrograph, the black sections represent the cells (filled with epoxy) and white sections the cell walls of the close-packed glass particles. The partial foam structure seen in Fig. 10(b) also proves an efficient bonding between the carboxyl groups of CMC and the surfaces of glass particles, which holds the particles together in the foam structure.

The SEM image of the fracture surface of a foam sample made from the medium size powder slurry with 60 wt% solid and 4 wt % of CMC and sintered at 750 °C for 30 min is shown in Fig. 11 (a). As is shown by the arrows in the same figure, the fractured and intact cell walls and edges accommodate both small and large sizes of pores. These pores are likely resulted from the partial bonding of the glass particles. The number and sizes of these cell wall/edge pores increase in the foam samples sintered at a lower temperature of 700 °C for 30 min (Fig. 11(b)). And as opposite, the thicker cell walls are seen in Fig. 11(c) in a foam sample sintered at 750 °C for a longer sintering time, 60 min. On the denser cell walls, the cleavage type of fracture as similar with the fracture of bulk glass is also clearly seen in Fig. 11(c). These further prove the effect of both sintering temperature and time on the final cell structure of the sintered foam samples.

The microscopic studies on the foam samples sintered at 650 °C showed a weak bonding between the particles, while the foam samples sintered at 800 °C resulted in excessive shrinkage due to the melting of glass particles. The foam samples made from the medium size powder slurry with 55 wt% of solid and 4 wt% of CMC and sintered at 700 and 750 °C had the final densities of between 400 and 405 kg m^{-3}. The final densities of the foam samples made from the same slurries with 60 wt% of solid and sintered at the same temperatures and sintering time were between 490 and 530 kg m^{-3}. The final density of foam sample made from the medium size powder slurry with 60 wt% of solid and 4 wt% of CMC was 500 kg m^{-3} when the sintering time increases to 60 min at 750 °C. Fig. 12 shows the quasi-static compression stress–strain curves of the foam samples of the medium powder slurries (55 and 60 wt% of solid) sintered at different temperatures and times. The initial peak stress in these stress–strain curves is taken as the compressive strength as shown in Fig. 12. The foam samples sintered at 700 °C for 30 min show relatively low compressive strengths, ~0.2 MPa. When the sintering temperature increases to 750 °C, the strength increases above 0.5 MPa. Increasing sintering time to 60 min for the foam sample of 60 wt% of solid increases the average compressive strength to 1.5 MPa. These confirm that both sintering temperature and time are effective in increasing the compressive strength. The tested foam samples fail

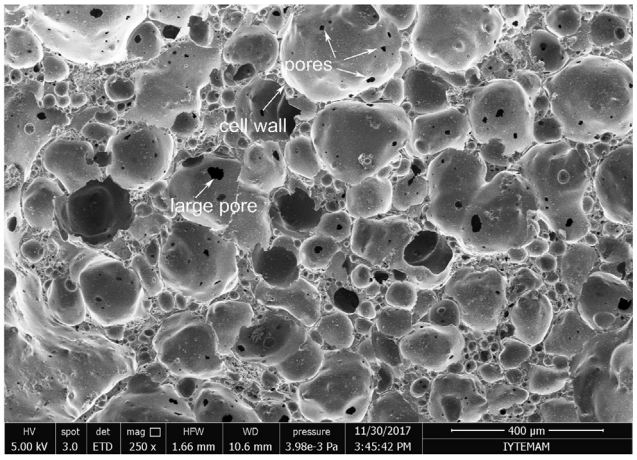

(a)

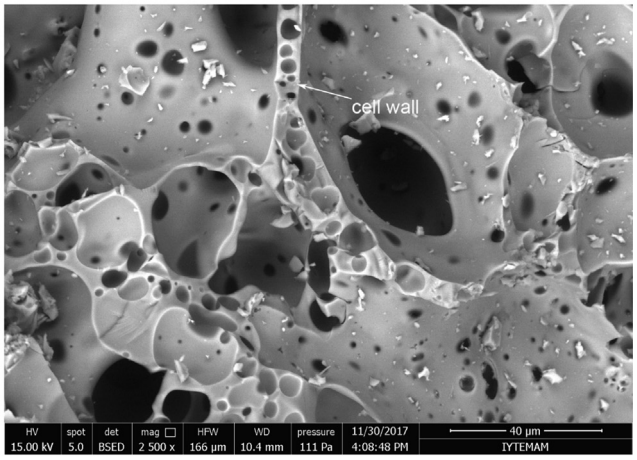

(b)

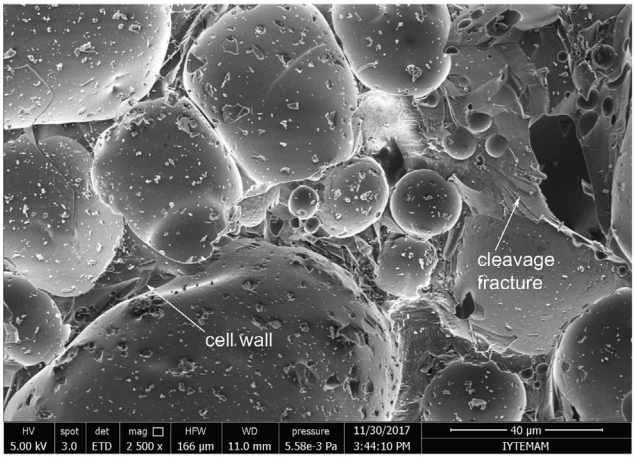

(c)

Fig. 11. The SEM images of the foam samples made from the slurries with 60 wt% of solid and sintered at (a) 750 °C for 30 min, (b) 700 °C for 30 min and (c) 750 °C for 60 min, showing fractured cell walls.

by forming cracks starting at the top or bottom of compression test plate. After initial cracking corresponding to the compressive strength, the fractured foam sample was re-compressed continuously until about large strains.

The thermal conductivities of foam samples made from the slurries of 55 and 60 wt% of solid and sintered at 750 °C for 30 min were measured. The thermal conductivities of the foam samples were measured 0.042 and 0.057 W m^{-1} K^{-1} at the densities of ~400 and ~500 kg m^{-3}, respectively.

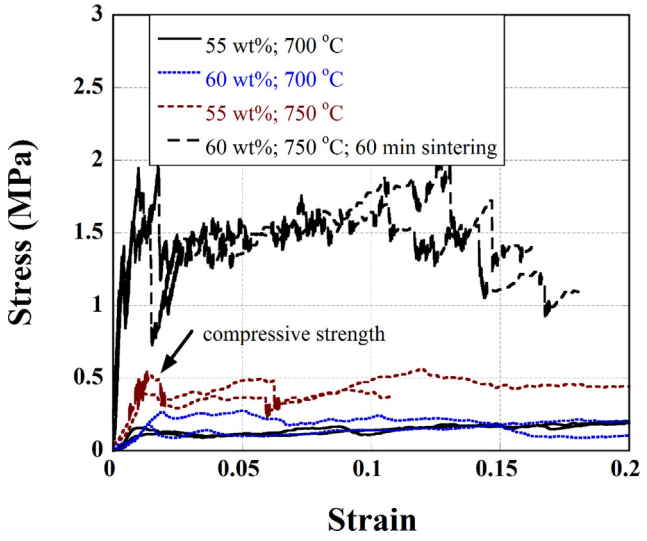

Fig. 12. The compression stress–strain curves of foam samples of 55 and 60 wt% solid content sintered at 700 and 750 °C for 30 and 60 min.

4. Discussion

A rapid increase in the viscosities of the powder slurries after about 50 wt% of solid has been shown previously [32–35]. The rapid increase in the viscosity is particularly seen in the fine powder size slurries with 60 wt% of solid content (Fig. 5(a-c)). The expansions of the slurries are shown to depend on the viscosity or the solid content of the slurries (Fig. 7(a-c)). Fig. 13 shows the variations of the bubble diameter and the number of cells, determined from camera records, with the foaming time. As is seen in the same figure, the number of cells of the slurries with 55 and 60 wt% of solid are higher than that of the slurry with 50 wt% of solid below 500 s; thereafter, the number of cells decreases more sharply and the cell diameter increases more rapidly in the slurries

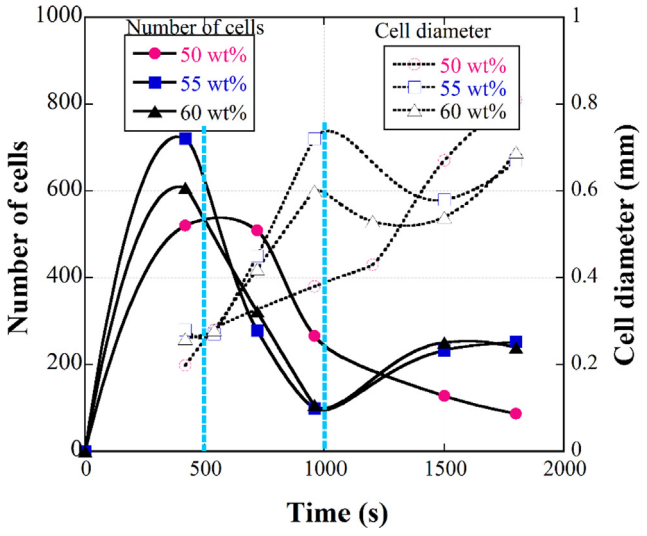

Fig. 13. The variations of the cell diameters and number of cells (from the surfaces of the mold) of the slurries with 50, 55 and 60 wt% of solid and 4 wt% of CMC as function of foaming time.

with 55 and 60 wt% of solid. These are also in accord with high initial expansion rates and rapid reductions of the expansions after maximum expansion in the slurries with 55 and 60 wt% of solid. The pressure difference between bubbles and slurry matrix increases with increasing viscosity. The increase in the internal pressure of bubbles may also results in a sudden, explosive-type of expansion [36]. The increased initial expansion rate of the slurries with the high solid content are likely due to this effect. However, the increase in the internal bubble pressure may also accelerate cell coarsening or decay. The increased extent of foam coarsening in the slurries with high viscosities has also been reported in previous studies [37–39]. The effect of water-solid ratio on the aerated concrete, using an Al powder foaming agent, was shown the most effective process parameter on the final density [40]. Furthermore, the addition of CMC stabilizes the slurries sterically and increases the viscosity due to the increased number of carboxymethyl groups binding the hydroxyl group.

The mechanisms of aluminum powder dissolution in calcium hydroxide solution was previously investigated and proposed to proceed by two sequential/parallel stages: aluminum oxide passive layer dissolution (activation) and aluminum hydration [41]. First, the passive layer Al_2O_3 reacts with water and forms AlOOH, then an amorphous $Al(OH)_3$ layer which releases $Al(OH)_4^-$ ion in strong alkali solutions. $Al(OH)_4^-$ ion reacts with Ca^{2+} ion and water, leading to the formation and the growth of katoite ($Ca_3Al_2(OH)_{12}$) as

$$3Ca^{2+} + 2Al(OH)_4^- + 8H_2O \leftrightarrow Ca_3Al_2(OH)_{12} + 6H_2(g) \quad (2)$$

The hydration reaction of aluminum occurs in stage 2, after the dissolution of the surface oxide layer by the following reaction

$$Al(s) + 3H_2O \leftrightarrow Al(OH)_3(s) + 3/2H_2(g) \quad (3)$$

Above reaction releases hydrogen gas and forms whisker-shape insoluble $Al(OH)_3$ and polycrystalline katoite crystals [41]. The crystal phase formation during foaming process may affect, depending on the size, by the amount and type of phases, the expansion behavior of slurries and the sintering behavior of foamed slurries. The XRD analysis of sintered foam bodies showed no crystal phase formation. This might be a result of low concentration of Ca(OH) added to the slurries.

The compressive strengths of the previously investigated glass foams [3,5,15,17,19,20,42–51] are shown in Fig. 14(a) as function of density, together with those of present study. The compressive strength vs. density data in Fig. 14(a) were fitted with the following Equation given for brittle ceramic foams [52],

$$\sigma_f = \sigma_s[C(\varnothing\rho_{rel})^{\frac{3}{2}} + (1-\varnothing)\rho_{rel}] \quad (4)$$

where, σ_s is the strength of glass, which was taken as 70 MPa [23], C is a constant, ρ_{rel} is the relative density of foam ($\frac{\overline{\rho}}{\rho_s}$, where $\overline{\rho}$ is the density of the foam and ρ_s is the density of the solid) and $\varnothing$ is the volume fraction of the solids contained on plateau borders. The first term in above equation is due to the bending and the second is due to the membrane stretching of cells. Eqn. (4) predicts the compressive strengths of open-cell foams when $\varnothing$ equals to 1, and the compressive strengths of closed cell foams when $\varnothing$ equals to 0. The compressive strengths of the reported glass foams are well fitted with $\varnothing$ values between 0.7 and 1 for the foam densities up to 300 kg m^{-3} and $\varnothing$ values between 0.7 and 0.9 for the foam densities between 300 and 600 kg m^{-3} (Fig. 14(a)). The tested present glass foam samples show however lower compressive strengths than those of previous studies. The compressive strengths however show well-match with those of open cell foams. The lower strength of present foams simply arises from the porosities on the cell edges and cell walls and partly from the anisotropy introduced during drying and sintering. The cells are elongated to the transverse to the foaming direction, resulting in a lower strength in this direction.

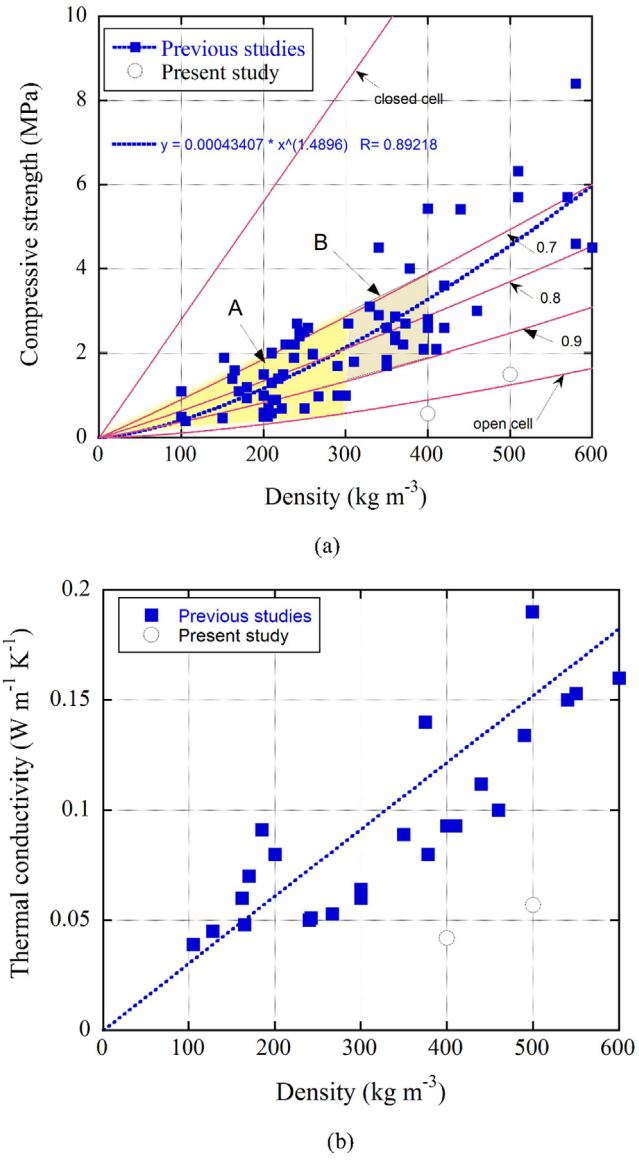

Fig. 14. (a) The variations of the (a) compressive strength and (b) thermal conductivity with the density of the glass foams of previous and present study.

Thermal conductivities of the glass foam samples reported previously as a function of density [3,43,49,53–55] are shown in Fig. 14(b) for the foam densities up to 600 kg m^{-3} together with the thermal conductivities of glass foams of present study. Thermal conductivities of tested foam glass range between 0.042 and 0.057 W m^{-1} K^{-1}. The tested foam glass, as shown in Fig. 14(b), exhibit lower thermal conductivities than those of the foam glasses reported in the literature. The relatively lower thermal conductivities of the present glass foams can be attributed to the smaller pore sizes and open cell structure of the tested glass foams.

5. Conclusions

The rheology of the recycled soda-lime glass powder slurries with 50, 55 and 60 wt% of solid and 0–4 wt% of CMC (binder) were studied experimentally. The slurries were expanded using an aluminum powder as foaming agent (0.75 wt%) and a calcium hydroxide as an activator (1 wt%). The green bodies of the foams of the selected glass powder slurries were sintered at temperatures between 650 and 800 °C for 30 and 60 min. Rheological studies

have shown that the slurries with 50 and 55 wt% of solid exhibited Newtonian behavior, while those with 60 wt% of solid non-Newtonian behavior. The apparent viscosities of the slurries increased with increasing the wt% of CMC, while the increase was more pronounced in the fine powder slurries. In relatively low-viscosity slurries, the initial expansion rate was slower and the expansions remained almost constant after the maximum expansion. The bursting of gas bubbles in the high-viscosity slurries led to higher initial expansion rates followed by abrupt reductions in expansions after the maximum expansion. The maximum expansions of the slurries increased from 300 to 350% when the viscosity increased to 5 Pa s. Above this critical viscosity, the maximum expansions were almost constant and over 400% until about 50 Pa s, above which the slurries became very thick to be expanded. The foam samples made from the slurries with 55 wt% and 60 wt% of solid and sintered at 700 °C and 750 °C for 30 min resulted in average densities between 355 and 530 kg m^{-3} and average compressive strengths between 0.2 and 0.5 MPa. Increasing sintering time from 30 min to 60 min at 750 °C increased the average compressive strength from 0.5 to 1.5 MPa for the foams made from the slurries with 60 wt% of solid. The thermal conductivity of sintered foam samples at 355 kg m^{-3} density was 0.042 W m^{-1} K^{-1}, while it increased to 0.057 W m^{-1} K^{-1} for the sintered foams at the density of 504 kg m^{-3}. The investigated foam glass samples exhibited lower compressive strength and thermal conductivities than foam glasses reported in the literature, which has been attributed to the small size of the porosities on the cell edge and walls and partly from introduced anisotropy during drying and sintering.

CRediT authorship contribution statement

Doğuş Zeren: Investigation, Formal analysis, Writing - original draft. **Ufuk Şentürk:** Methodology, Writing - review & editing. **Mustafa Güden:** Conceptualization, Writing - review & editing, Supervision.

Declaration of Competing Interest

The authors declare that they have no known competing financial interests or personal relationships that could have appeared to influence the work reported in this paper.

Acknowledgments

The authors would like to thank AKG Gazbeton of Turkey for providing foaming agent and lime for the expansion experiments.

References

[1] B. Long, Glass product and method of manufacturing sponge-like glass, Saint Gobain (1934).
[2] B. Long, Process for the manufacture of multicellular glass, Google Patents (1938).
[3] Wrap, www.wrap.org.uk, 2011.
[4] E. Bernardo, F. Albertini, Glass foams from dismantled cathode ray tubes, Ceram. Int. 32 (6) (2006) 603–608.
[5] H.R. Fernandes, D.U. Tulyaganov, J.M.F. Ferreira, Production and characterisation of glass ceramic foams from recycled raw materials, Adv. Appl. Ceram. 108 (1) (2009) 9–13.
[6] B. Chen, K.Q. Wang, X.J. Chen, A.X. Lu, Study of foam glass with high content of fly ash using calcium carbonate as foaming agent, Mater. Lett. 79 (2012) 263–265.
[7] H.R. Fernandes, D.U. Tulyaganov, J.M.F. Ferreira, Preparation and characterization of foams from sheet glass and fly ash using carbonates as foaming agents, Ceram. Int. 35 (1) (2009) 229–235.
[8] R.R. Petersen, J. König, M.M. Smedskjaer, Y. Yue, Foaming of CRT panel glass powder using Na2CO3, Glass Technol.-Eur. J. Glass Sci. Technol. Part A 55 (1) (2014) 1–6.
[9] Y.C. Liao, C.Y. Huang, Glass foam from the mixture of reservoir sediment and Na2CO3, Ceram. Int. 38 (5) (2012) 4415–4420.
[10] R.R. Petersen, J. König, Y. Yue, The mechanism of foaming and thermal conductivity of glasses foamed with MnO2, J. Non-Cryst. Solids 425 (2015) 74–82.
[11] J. Konig, R.R. Petersen, Y.Z. Yue, D. Suvorov, Gas-releasing reactions in foam-glass formation using carbon and MnxOy as the foaming agents, Ceram. Int. 43 (5) (2017) 4638–4646.
[12] A.I. Shutov, L.I. Yashurkaeva, S.V. Alekseev, T.V. Yashurkaev, Study of the structure of foam glass with different characteristics, Glass Ceram. 64 (9–10) (2007) 297–299.
[13] F. Mear, P. Yot, M. Ribes, Effects of temperature, reaction time and reducing agent content on the synthesis of macroporous foam glasses from waste funnel glasses, Mater. Lett. 60 (7) (2006) 929–934.
[14] D.U. Tulyaganov, H.R. Fernandes, S. Agathopoulos, J.M.F. Ferreira, Preparation and characterization of high compressive strength foams from sheet glass, J. Porous Mater. 13 (2) (2006) 133–139.
[15] J.P. Wu, A.R. Boccaccini, P.D. Lee, M.J. Kershaw, R.D. Rawlings, Glass ceramic foams from coal ash and waste glass: production and characterisation, Adv. Appl. Ceram. 105 (1) (2006) 32–39.
[16] H.W. Guo, Y.X. Gong, S.Y. Gao, Preparation of high strength foam glass-ceramics from waste cathode ray tube, Mater. Lett. 64 (8) (2010) 997–999.
[17] J. Garcia-Ten, A. Saburit, M.J. Orts, E. Bernardo, P. Colombo, Glass foams from oxidation/reduction reactions using SiC, Si3N4 and AlN powders, Glass Technol.-Eur. J. Glass Sci. Technol. Part A 52 (4) (2011) 103–110.
[18] F. Mear, P. Yot, M. Cambon, A.M. Ribes, Elaboration and characterisation of foam glass from cathode ray tubes, Adv. Appl. Ceram. 104 (3) (2005) 123–130.
[19] Y. Attila, M. Guden, A. Tasdemirci, Foam glass processing using a polishing glass powder residue, Ceram. Int. 39 (5) (2013) 5869–5877.
[20] A.S. Llaudis, M.J.O. Tari, F.J.G. Ten, E. Bernardo, P. Colombo, Foaming of flat glass cullet using Si3N4 and MnO2 powders, Ceram. Int. 35 (5) (2009) 1953–1959.
[21] S.É. Ivanov, A.V. Belyakov, Diatomite and its applications, Glass Ceram. 65 (1) (2008) 48–51.
[22] H.R. Femandes, D.U. Tulyaganov, J.M.F. Ferreira, Preparation and characterization of foams from sheet glass and fly ash using carbonates as foaming agents, Ceram. Int. 35 (1) (2009) 229–235.
[23] E. Bernardo, R. Cedro, M. Florean, S. Hreglich, Reutilization and stabilization of wastes by the production of glass foams, Ceram. Int. 33 (6) (2007) 963–968.
[24] R.R. Petersen, J. Konig, Y.Z. Yue, The viscosity window of the silicate glass foam production, J. Non-Cryst. Solids 456 (2017) 49–54.
[25] Y.A. Spiridonov, L.A. Orlova, Problems of Foam Glass Production, Glass Ceram. 60 (9–10) (2003) 313–314.
[26] V.E. Manevich, K.Y. Subbotin, Foam glass and problems of energy conservation, Glass Ceram. 65 (3–4) (2008) 105–108.
[27] N. Narayanan, K. Ramamurthy, Structure and properties of aerated concrete: a review, Cem. Concr. Compos. 22 (5) (2000) 321–329.
[28] A.J. Hamad, Materials, Production, Properties and Application of Aerated Lightweight Concrete: A Review, International, J. Mater. Sci. Eng. 2 (2) (2014) 152–157.
[29] G. Bumanis, D. Bajare, J. Locs, A. Korjakins, Alkali-silica reactivity of foam glass granules in structure of lightweight concrete, Constr. Build. Mater. 47 (2013) 274–281.
[30] X.L. Qu, X.G. Zhao, Previous and present investigations on the components, microstructure and main properties of autoclaved aerated concrete – a review, Constr. Build. Mater. 135 (2017) 505–516.
[31] G. Kastiukas, X.M. Zhou, K.T. Wan, J.C. Gomes, Lightweight Alkali-Activated Material from Mining and Glass Waste by Chemical and Physical Foaming, J. Mater. Civ. Eng. 31 (3) (2019) 8.
[32] H. Eilers, Die Viskosität von Emulsionen hochviskoser Stoffe als Funktion der Konzentration, Kolloid-Zeitschrift 97 (3) (1941) 313–321.
[33] V. Vand, Viscosity of Solutions and Suspensions. II. Experimental Determination of the Viscosity-Concentration Function of Spherical Suspensions, J. Phys. Colloid Chem. 52 (2) (1948) 300–314.
[34] D. Prasad, H.K. Kytömaa, Particle stress and viscous compaction during shear of dense suspensions, Int. J. Multiph. Flow 21 (5) (1995) 775–785.
[35] E. Koos, E. Linares-Guerrero, M.L. Hunt, C.E. Brennen, Rheological measurements of large particles in high shear rate flows, Phys. Fluids 24 (1) (2012) 013302.
[36] A.B.J. Kroezen, J.G. Wassink, C.A.C. Schipper, The flow properties of foam, 104 (10) (1988) 393-400.
[37] C. Koerner, Physics of Foaming, Integral Foam Molding of Light Metals, Springer, Berlin Heidelberg, 2008, pp. 77–102.
[38] P. Sepulveda, J.G.P. Binner, Processing of cellular ceramics by foaming and in situ polymerisation of organic monomers, J. Eur. Ceram. Soc. 19 (12) (1999) 2059–2066.
[39] A.D. Ronteltap, B.R. Damsté, M. De Gee, A. Prins, The role of surface viscosity in gas diffusion in aqueous foams. I. Theoretical, Colloids Surf. 47 (1990) 269–283.
[40] Y.-L. Chen, J.-E. Chang, Y.-C. Lai, M.-I.M. Chou, A comprehensive study on the production of autoclaved aerated concrete: effects of silica-lime-cement composition and autoclaving conditions, Constr. Build. Mater. 153 (2017) 622–629.
[41] S. Kanehira, S. Kanamori, K. Nagashima, T. Saeki, H. Visbal, T. Fukui, K. Hirao, Controllable hydrogen release via aluminum powder corrosion in calcium hydroxide solutions, J. Asian Ceram. Soc. 1 (3) (2013) 296–303.

[42] A.I. Shutov, L.I. Yashurkaeva, S.V. Alekseev, T.V. Yashurkaev, Modeling of the structure of heat-insulating foam glass, Glass Ceram. 64 (11–12) (2007) 397–399.
[43] O.V. Kaz'mina, V.I. Vereshchagin, A.N. Abiyaka, Prospects for use of finely disperse quartz sands in production of foam-glass crystalline materials, Glass Ceram. 65 (9–10) (2008) 319–321.
[44] O.V. Kaz'mina, V.I. Vereshchagin, A.N. Abiyaka, Assessment of the compositions and components for obtaining foam-glass-crystalline materials from aluminosilicate initial materials, Glass Ceram. 66 (3–4) (2009) 82–85.
[45] E. Bernardo, G. Scarinci, P. Bertuzzi, P. Ercole, L. Ramon, Recycling of waste glasses into partially crystallized glass foams, J. Porous Mater. 17 (3) (2010) 359–365.
[46] M.S. Garkavi, O.K. Mel'chaeva, A.I. Nazarova, Effect of the process parameters of mix preparation on the properties of foam glass, Glass Ceram. 68 (1–2) (2011) 44–46.
[47] J.G. Bai, X.H. Yang, S.C. Xu, W.J. Jing, J.F. Yang, Preparation of foam glass from waste glass and fly ash, Mater. Lett. 136 (2014) 52–54.
[48] J.L. Bian, W.L. Cao, L. Yang, C.Q. Xiong, Experimental research on the mechanical properties of tailing microcrystalline foam glass, Materials 11 (10) (2018) 19.
[49] C.P. Xi, F. Zheng, J.H. Xu, W.G. Yang, Y.Q. Peng, Y. Li, P. Li, Q. Zhen, S. Bashir, J.L. Liu, Preparation of glass-ceramic foams using extracted titanium tailing and glass waste as raw materials, Constr. Build. Mater. 190 (2018) 896–909.
[50] B.S. Semukhin, O.V. Kazmina, A.Y. Volkova, V.I. Suslyayev, Physical characteristics of foam glass modified with zirconium dioxide, Russ. Phys. J. 59 (12) (2017) 2130–2136.
[51] W.L. Huo, S. Yan, J.M. Wu, J.J. Liu, Y.G. Chen, Y.N. Qu, X.Y. Tang, J.L. Yang, A novel fabrication method for glass foams with small pore size and controllable pore structure, J. Am. Ceram. Soc. 100 (12) (2017) 5502–5511.
[52] L.J. Gibson, M.F. Ashby, Cellular Solids: Structure and Properties, 2nd ed., Cambridge University Press, Cambridge, 1997.
[53] F. Mear, P. Yot, R. Viennois, M. Ribes, Mechanical behaviour and thermal and electrical properties of foam glass, Ceram. Int. 33 (4) (2007) 543–550.
[54] N.M. Bobkova, S.E. Barantseva, E.E. Trusova, Production of foam glass with granite siftings from the Mikashevichi deposit, Glass Ceram. 64 (1) (2007) 47–50.
[55] J. Konig, R.R. Petersen, N. Iversen, Y.Z. Yue, Suppressing the effect of cullet composition on the formation and properties of foamed glass, Ceram. Int. 44 (10) (2018) 11143–11150.